Third Joint Eurohaptics Conference and Symposium on Haptic Interfaces
for Virtual Environment and Teleoperator Systems
Salt Lake City, UT, USA, March 18-20, 2009

Ergonomics of Exoskeletons: Objective Performance Metrics

André Schiele

European Space Agency, Mechanical Engineering Department, Automation & Robotics Section

ABSTRACT

In this paper it is shown how variation of the kinematic structure of an exoskeleton and variation of its fixation strength on the human limb influences objective task performance metrics, such as interface load, tracking error and voluntary range of motion in a signal tracking experiment.
It is shown that interface forces of up to 230 N and torques of up to 1.46 Nm can be created purely stemming from joint misalignments between exoskeleton and human limbs. Such joint misalignments can reach up to ± 10 cm during movement, even if both systems were initially well aligned. Interface forces are shown to be responsible for a workspace reduction. By estimation of a physical human-robot interaction model, it will be shown quantitatively how interface forces relate to the geometrical mismatches between human limb and exoskeleton. Parameter estimation has been used to determine the attachment stiffness of 273 N/m ± 46 N/m from measured data of 14 test subjects.
An exoskeleton kinematic structure with passive compensation joints is shown to significantly reduce interface loading on the human arm.

KEYWORDS: Exoskeleton, ergonomics, physical human robot interaction, attachment stiffness, interface forces.

1 INTRODUCTION

Exoskeletons are subject to intense interest and research at this point in time, for a large field of applications that spans from haptics and fundamental haptic device research [1] over bilateral tele-robotics [2] and defence applications [3], up to the relatively new field of robotic physical therapy [4]. All types of wearable robots must be safe, comfortable and able to smoothly interact with the human user. Safe physical human-robot interaction (pHRI) is difficult to achieve and to quantify and therefore is still a relatively new and important area of research in the field of robotics [5].
Two of the most important aspects influencing comfort and safety in wearable robots, are the actuation & control, and the kinematic design of the movable structure. Up to now, many researchers published novel actuation concepts such as compliant drives or antagonist actuators, as well as advanced control architectures that help to improve the safety of human-machine interaction for wearable robots substantially.
An area however, to which less attention has been paid, is the mechanical and kinematic design of wearable robots, for optimal pHRI. Each exoskeleton designer optimizes his devices according to some personal understanding or experience of what is required. Yet, the difficulty of aligning the principal axes of motion correctly between human joints and exoskeleton joints is known. It is also known that all types of kinematic offsets between human and robot create disturbance forces (sometimes also called interface or interaction forces) at the human-robot interface. However, currently no investigation known to the author has quantified typical magnitudes of such loads, has explained their exact causes and characteristics or has shown how such force artefacts influence objective and subjective performance in typical exoskeleton applications.
In our line of research [6], we aim to develop a mechanically transparent exoskeleton haptic device, that limits the creation of interface forces and is more ergonomic. We intend to develop an exoskeleton that is robust to misalignment and thus, can be used by a large range of operators without requiring adjustments. This requirement stems from the need to be a haptic interface for Astronaut crew inside the International Space Station. We have presented a novel design paradigm for human centered exoskeleton kinematics in [7], which postulates the need for passive compensatory joints inside the kinematic mechanism of an exoskeleton. We have also presented and validated an analytical pHRI-model in [8], which allows to relate geometric attachment properties such as joint center of rotation offsets, the attachment stiffness and the kinematic design parameters (Denavit-Hartenberg Parameters) of the exoskeleton to the creation of interface loads.
It is the goal of this paper to quantify, for the first time, the magnitudes of (1) offsets that can be created between human and exoskeleton joints during typical movements, of (2) typical interface loads and of (3) the attachment stiffness apparent in a typical tracking task with an exoskeleton. Moreover, it is the goal of this paper to analyze the effect of including/excluding passive compensatory joints in an exoskeleton on objective performance metrics. The influence of variation of attachment stiffness on objective performance metrics shall be shown as well. The objective metrics investigated in this paper are, (1) interface load on the human arm, (2) tracking error and (3) available range of motion. Influence of the experiment parameters on subjective performance and their relation to objective metrics is reported in greater depth in [6].
As such, the presented experiment and results will help to analyze whether the ergonomics of exoskeletons can be improved by optimal attachment parameters and kinematic structure.

2 METHOD

In order to quantify the effects of misalignment and attachment pressure on interface force generation, an experiment was conducted with 14 test subjects. All subjects were asked to track a target signal on a computer screen with an exoskeleton structure attached to their elbow. The control signal was commanded by the elbow joint of the exoskeleton interface. The settings of the exoskeleton were varied by an experimenter between runs, as will be explained below.

2.1 Theoretical pHRI model

In order to help the reader understand the identification procedure carried out below, the essentials of an analytical single degree-of-freedom (d.o.f.) physical human-robot interaction (pHRI) model

ESA/ESTEC, Keplerlaan 1, 2201 AZ Noordwijk, The Netherlands, E-mail: Andre.Schiele@esa.int

are briefly outlined. The model was already presented in [8]. The single d.o.f. model relates the geometric attachment parameters between an exoskeleton and a human joint to the interface force F_d, according to:

$$F_d = k \cdot d_{tot}(\beta, x, y, l_{ex}, z_{ex}) \quad (1)$$

Where, k denotes the interface stiffness and d_{tot} the total displacement of the distal attachment cuff along the limb during motion. The total displacement is formulated as a function of β, the exoskeleton's main joint angle, the offsets x and y between the human limb centre of rotation ICR_h and exoskeleton main joint centre of rotation CR_e (both in parent-link coordinate frame), and the Denavit-Hartenberg parameters of the exoskeleton, l_{ex} (link lenght) and z_{ex} (link offset). A graphical illustration of the model and its geometric parameters is depicted in Figure 1.
This model is used to estimate the existing joint centre of rotation offsets and attachment stiffness for each experiment. Input to the non-linear parameter identification is the measured interface force between exoskeleton and human limb. To measure offsets and interface stiffness directly would be exceedingly complex without this functional identification.

2.2 Hardware Setup

For the experiments, the subjects wore the elbow articulation of the ESA EXARM exoskeleton [9]. The mechanical structure of the exoskeleton features three joints for interaction with the elbow. The device is fixed by means of two inflatable air-cushions on the subject's upper- and forearm and is balanced by a counter-mass system attached via cables.
Joint Θ_7 is the primary elbow joint of the exoskeleton. Before each experiment run, this joint was aligned to match the subject's elbow flexion axis as good as possible. This was done by pure visual alignment and some trial movements. Joint Δ_8 is a linear offset compensation joint and joint Θ_9 is a rotary offset compensation joint. An overview of the exoskeleton articulation worn by a subject is shown in Figure 2.
In this experiment, it was possible to alter the mechanical structure of the exoskeleton. It could be swapped from a seemingly ergonomic design to a conventional one by locking the compensation joints Δ_8 and Θ_9. All three joints of the device are equipped with high-precision potentiometers to directly measure the joint displacements β of joint Θ_7, *dlin* of Δ_8 and Θ_{rot} of joint Θ_9.

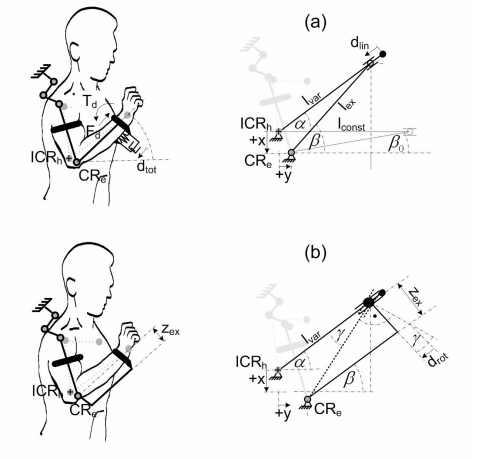

Figure 1. Overview of the pHRI-model used for identification of the geometric parameters from measured interface force data.

Furthermore, a 6 d.o.f. force/torque sensor is integrated near the forearm attachment cuff (ATI Nano Series). It is used to directly measure the created interface force F_d between human and exoskeleton during the experiment. Furthermore, the interface moment T_d around an axis passing through compensation joint Θ_9 is measured directly. The signs of force and torque correspond to the directions shown in Figure 1 (a).

2.3 Experiment Protocol

The 7 male and 7 female subjects (stature 1.75 m ± 0.09 m, mass: 68.7 kg ± 12.8 kg) were asked to follow a random multisine signal v with a frequency content ranging from 0.05 – 0.35 Hz. This target signal was displayed on a computer screen by a moving blue bar. The subjects were able to track the movement of the bar by moving their elbow inserted into the exoskeleton. The angle β on the exoskeleton joint Θ_7 was measured and controlled a second bar (green), which was displayed below the target signal on the computer screen. To provide some visual feedback of the goodness of the tracking performance, a red bar showed the instantaneous tracking error. The target signal v demanded elbow movement from 0 – 90 Deg. flexion. Each experiment run took exactly 60 s. The three potentiometers on the exoskeleton, as well as the force signals were measured at a rate of 1 kHz. Analog filters were used to limit measurement noise to below the quantization level of the AD converters (12bit).
Between runs, the attachment stiffness on the exoskeleton's upper and forearm air-cushions was randomly varied by the experimenter. By inflating/deflating the air-cushions, the experimenter was able to vary the air-cushion pressure from 10 – 60 mmHg, in steps of 10 mmHg. Also, the kinematic setting of the exoskeleton was randomly changed between runs. The experimenter varied the kinematic exoskeleton structure between *locked (L)* and *free/unlocked (U)* settings. In the *U* setting, the passive joints were free to move, our seemingly more ergonomic design, while in *L* setting all passive compensation joints of the exoskeleton were blocked; thus, emulating a non-ergonomic design. Each combination of factors was tested once per subject in random order, which resulted in 12 experiment trials per subject.
All subjects were blinded to the experiment conditions. The signal tracking motion was carried out with the arm elevated in a horizontal plane, to further reduce effects of gravity on the measured interface loads.

2.4 Statistical Design

Statistical hypothesis testing revealed the influence of the kinematic setting variation and attachment pressure variation to the objective performance measures, the dependent variables.

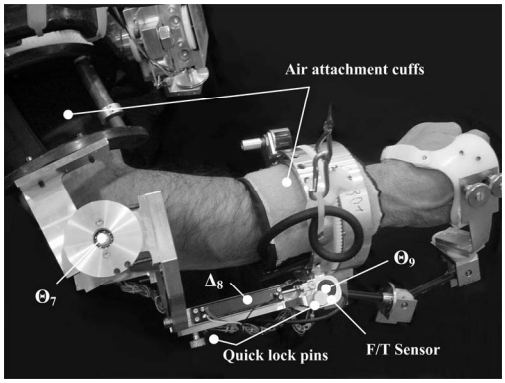

Figure 2. Overview of the exoskeleton's elbow articulation that was used to control the tracking signals in the presented experimental study.

Statistical hypothesis testing was done by means of multi-way ANOVAs. Repetitions over the relevant independent variables were considered and also interaction between variables was analyzed. Due to the restricted length of this manuscript, not more detailed information on the employed statistical methods will be given. However, the p-value that was obtained from the relevant tests will be always quoted. In all following figures, significance between groups will be indicated graphically by asterisks according to following code: *, $p<0.05$; **, $p<0.01$; ***, $p<0.001$.

2.4.1 Independent variables

The two primary independent factors are: (1) the kinematic condition with the two levels '*locked*' *(L)* and '*unlocked*' *(U)* and (2) the interface pressure with the six levels ranging from 10 – 60 mmHg. In some hypothesis tests, also (3) the subjects were used as independent factor.

2.4.2 Dependent variables

The dependent variables were computed and analyzed for the group, as well as for the individual subjects. The dependent variables are (1) the mean absolute interaction force $|\overline{F}_d|$ per trial, (2) the mean absolute interaction torque $|\overline{T}_d|$ per trial, and (3) the RMS error of the signal tracking E_{Tr} per trial, defined as

$$E_{Tr} = \sqrt{\sum_{i=1}^{s} (\beta_i - \nu_i)^2 / s} \,, \qquad (1)$$

with ν_i, the angle of the multisine signal at the i-th sample, β_i the exoskeleton elbow angle at the i-th sample, and s the signal length in samples (s=60000).

In order to reveal the influence of the kinematic setting also during movement, five additional measures were processed into angle bins, per experiment. The binned dependent variables are (4) the raw, signed interaction Force $\overline{F}_{d\beta}$, (5) the raw, signed interaction Torque $\overline{T}_{d\beta}$, (6) the displacement of the linear compensation joint d_{lin}, and (7) the displacement of the rotary compensation joint Θ_{rot}. These variables were accumulated for each trial into 9 bins that each spanned 10 Deg. wide, over the exoskeleton elbow joint angle β (in the range from 0 – 90 Deg.).

Furthermore, the (8) voluntary range of motion R_β was derived from the exoskeleton elbow joint angle β. The voluntary range of motion is expressed in percent of multisine target angle v, that had been reached. It is defined as the ratio $(s_\beta \cdot 100)/s_v$, with s_β, the total number of samples for which β lies inside a 10 Deg. wide bin per trial, and s_v the total number of samples for which v lies within the same 10 Deg. wide bin. Thus, this measure tolerates samples that do not lie within the same bin at the same time and is therefore an indirect measure of the workspace that was used. It is thus independent of the tracking itself. This calculus had to be done since the true human elbow joint angle α (Figure 1 a) is not measurable directly.

3 RESULTS

3.1 Interface / Interaction Loading

3.1.1 Dependence on kinematic configuration for the Group

The interface load is sensitive to the kinematic configuration of the exoskeleton. In *locked* configuration, the exerted interface forces are higher than in *unlocked* configuration.

For the group, the peak-to-peak interaction forces F_d span from -232 – 165 N for the *L* and only from -57 – 70 N for the *U* condition, as shown in Figure 3 (a). The full spectrum of measured peak-to-peak interaction torques T_d spans from -1.0 – 1.46 Nm for the *L* configuration and only from -0.4 – 0.60 Nm for the *U* kinematic condition, as shown in Figure 3 (d). The absolute loading $|\overline{F}_d|$, and $|\overline{T}_d|$ over all experiment trials and subjects is shown in Figure 3 (b) and (e) and shows a difference over the *L* and *U* factors. The mean interaction force $|\overline{F}_d|$ (Figure 3 b) is lower in the *U* (14.02 ± 11.95 N) than in the *L* (17.75 ± 16.33 N) condition *(p<0.05)*, as well as the mean interaction torque $|\overline{T}_d|$ (Figure 3 e), that is also lower in the *U* (0.109 ± 0.099 Nm) than in the *L* (0.272 ± 0.153 Nm) condition *(p<0.001)*. The hypothesis testing for both loads has revealed that the subjects heavily contribute to the measured variance *(p<0.001)* and that the kinematic setting factor shows strong interaction with the subject factor *(p<0.001)*.

In Figure 3 (c) and (f) the interface load is shown over both, pressure variation and kinematic setting variation. It can be seen that the kinematic setting has the strongest impact on reducing interface torque $|\overline{T}_d|$ over all pressure increments. In order to analyze the reason why loads are lower in *U* than in *L* kinematic configuration of the exoskeleton, we will have a look at the load exertion over the workspace.

The binned interaction forces $\overline{F}_{d\beta}$, and torques $\overline{T}_{d\beta}$ are shown in Figure 4 over the exoskeleton elbow angle β. The standard deviation is shown as upper and lower bounds on each curve. It can be seen that the spread of force (Figure 4 a) and torque loads (Figure 4 b) is already smaller for the *U* configuration. The mean force exertion $\overline{F}_{d\beta}$ (Figure 4 a) is smaller for the *U* kinematic setting in the 85 Deg. angle bin *(p<0.01)*, and the exerted interaction torque $\overline{T}_{d\beta}$ (Figure 4 b) is lower in the *U* kinematic condition for the first six bins spanning from 0 to 60 Degrees *(p<0.001, p<0.05)*. The presented graphs indicate that the effect of the passive compensation joints is most optimal near the stroke ends. There, they act to remove peak loads.

Figure 4 (a) shows additionally the results from the parameter fit of the pHRI-model on the measured group data. The coefficient of determination (R^2 = 97.53 %), as well as the norm of the residuals (|*res.*|=3.45 N) indicate a good fit of the model to the measured data. The estimated pHRI-model parameters that have been identified from the mean force $\overline{F}_{d\beta}$ for the entire group are:

$$\hat{k}_G = 311.5 \text{ N/m}, \hat{x}_G = 0.0076 \text{ m}, \hat{y}_G = -0.097 \text{ m},$$
$$\hat{l}_{exG} = 0.167 \text{ m}, \hat{z}_{exG} = 0.13 \text{ m}.$$

Again, the kinematic setting factor shows strong interaction with the subjects for each bin and dependent variable *(p<0.001)*.

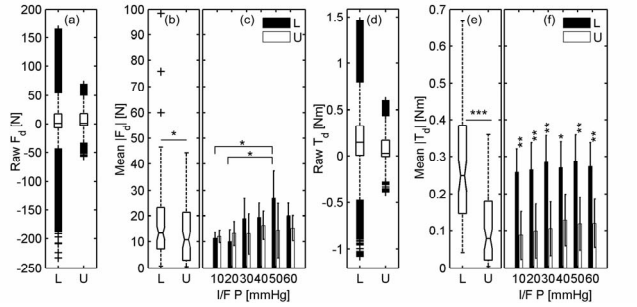

Figure 3. Boxplots and bar-graphs of the interface force $\overline{F}_d$ (a – c) and interface torque $\overline{T}_d$ (d – f) in dependence of kinematic condition (*L*: *passive joints locked, U*: *passive joints free to move)* and attachment pressure (10 – 60 mmHg).

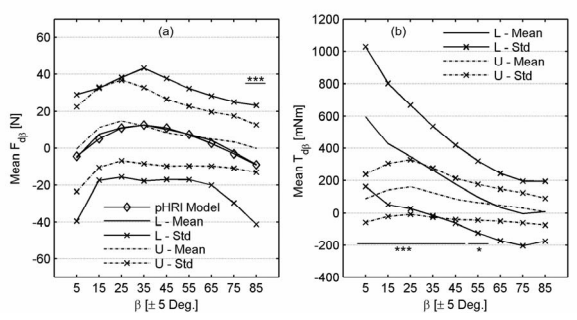

Figure 4. Binned interface force $\bar{F}_{d\beta}$ (a) and torque $\bar{T}_{d\beta}$ (b) over exoskeleton elbow angle, for both kinematic configurations. The p-HRI model fit is shown in (a).

3.1.2 Dependence on Kinematic Configuration for Individual Subjects

Due to the evident interaction between kinematic setting and subject factors in the interface load data, it is interesting to look at differences between individual subjects as well.

Figure 5 shows the effects of kinematic setting variation to the interaction loads per subject. The accumulated mean values of absolute force over all trials are shown per subject. Little bars indicate the 95% *CI* on correct estimate of the means. Four subjects experience less force $|F_d|$ in the *U* condition (Figure 5 a), while no subject experiences less force in the *L* condition. With respect to the interaction torque $|T_d|$ (Figure 5 b), the effect is even more pronounced, with 9 subjects experiencing less interaction torque in the *U* kinematic condition, and no subject that experiences less torque in the *L* condition.

This underlines both facts that we have seen so far; (1) the kinematic condition with additional passive joints causes less interface loading, and, (2) different subjects react differently to the exoskeleton's kinematic configuration change. What could be the reason for this dependence on the subjects?

An answer can be provided by analyzing the measured interface force data by means of parameter identification with the pHRI-model. Logically, the data from the *L* data-sets has been used. The offset estimates $\hat{x}$, $\hat{y}$, as well as the estimated attachment stiffness $\hat{k}$ are shown per subject in Table 1. The table also shows the coefficient of determination R^2 and the norm of the residuals $|res.|$, to indicate the goodness of fit. Figure 6 depicts graphs of the model fits and the measured data in 2 Deg. wide bins over the exoskeleton elbow angle. The graphs are sorted according to the direction of the offsets that resulted from the parameter identification.

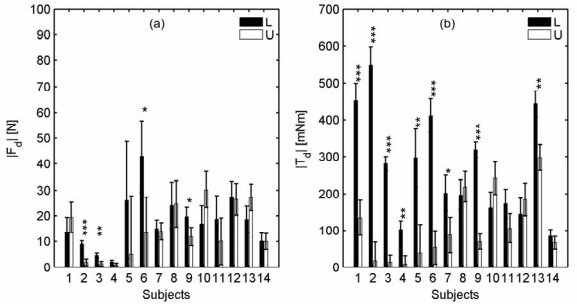

Figure 5. Bar-graphs of the absolute interface force $|\bar{F}_d|$ (a) and absolute interface torque $|\bar{T}_d|$ (b) for each subject in dependence of kinematic condition (*L*: *passive joints locked, U*: *passive joints free to move)*.

As explained in greater detail in [6], all combinations of offsets exhibit a particular and distinct trend of the interface loads.

It can be seen that despite the alignment of the exoskeleton to the subject's elbow axis prior to the experiment, some relatively large offsets have occurred during the experiment. Induced misalignments range from -2.2 to +13.6 cm for *x*-offsets and from -11.7 to +5.9 cm for *y*-offsets. The main reason for these relatively large values must have been induced slip and an amplification of remaining initial alignment offsets during elbow movement.

It is interesting to observe that all subjects that feature offsets in $+x$ and $+y$ direction, experience a profound reduction of interface force, while the others don't experience a similarly profound effect.

This fact explains the interaction terms and even opens the way to optimize the kinematic structure of the exoskeleton interface that has been used. Depending on the combination of offsets, the passive joints worked better or worse. In particular for those Subjects who experienced joint center offsets in $+x$ and $+y$ direction, the compensation joints worked optimal. For them, force pointed mostly in positive, proximal direction (Figure 6 a) towards larger joint angles. This is where the peak forces are caused. That must mean in turn, that the linear passive joint needs an up-dated range towards proximal direction to function better also for the other subjects.

In the course of this paper we will not go further into detail, regarding analysis of the causes of variation between subjects. However, we note that the interaction terms apparent in the data can be explained and that the pHRI model can be used for exoskeleton design optimization.

Table 1: Identified pHRI-model parameters from measured interface forces, per subject (S: subject, $\hat{k}$: attachment stiffness, $\hat{x}$: x-offset, $\hat{y}$: y-offset, $\hat{l}$: link length, $\hat{z}$: link offset).

S.	$\hat{k}$ [N/m]	$\hat{x}$ [$\cdot 10^{-3}$ m]	$\hat{y}$ [$\cdot 10^{-3}$ m]	R^2 [%]	$\|res.\|$ [N]
1	251	-22.3	-78.9	89.2	17.7
2	249	68.4	18.6	98.9	5.2
3	222	48.2	58.5	97.3	5.1
4	249	2.1	2.1	21.6	6.3
5	256	124.4	-48.7	93.5	23.0
6	286	136.2	7.9	83.8	47.2
7	264	-17.2	-116.9	99.2	8.3
8	374	3.5	-87.7	98.6	11.2
9	237	78.3	10.3	66.4	26.0
10	250	1.8	-76.6	91.6	16.3
11	253	-15.0	-54.2	56.2	42.7
12	271	5.6	-77.1	94.5	15.9
13	373	-0.5	-81.3	98.4	8.1
14	284	25.2	-115.6	95.7	10.1

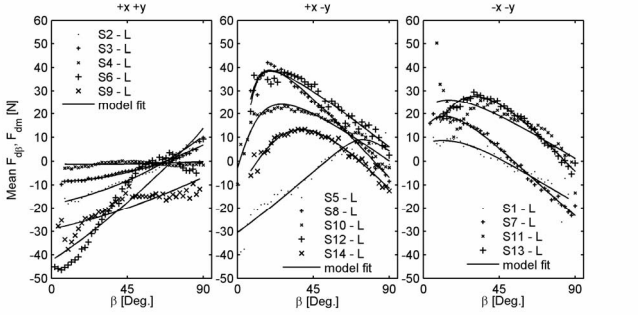

Figure 6. Raw interaction force measurements $\bar{F}_{d\beta}$ in 2 Deg. wide bins over the exoskeleton elbow angle β and model fit F_{dm} from pHRI-model, per subject sorted according to direction of joint centre of rotation offsets.

3.1.3 Dependence on Attachment Pressure

Interestingly, the interface load exerted between exoskeleton and the human limb is hardly influenced by variation of the attachment pressure on the exoskeleton's fixation cuffs. This is the case for the group and for individual subjects.

The bargraphs in Figure 3 (c) and (f) show the group means of the interaction loads over attachment pressure for both kinematic levels over all trials and subjects. Forces are depicted in (c) and torques in (f). Error bars indicate their 95 % *CI* on correct estimate of the means. Figure 3 (c) shows some difference between interface force levels of 10 & 20 mmHg with respect to 50 mmHg pressure *(both $p<0.05$)*, but no clear trend is visible, which makes this difference seem irrelevant.

3.2 Signal Tracking Performance

The RMS tracking error E_{Tr} for the subject group, over all trials, varies within 13.27 ± 2.8 Deg. A boxplot in Figure 7 (a) shows the entire spread of E_{Tr} measurement points. Overall, no clear effect can be associated with the kinematic setting variation or pressure variation alone. The statistical testing reveals that the subjects are the strongest contributors to the variability of the RMS tracking error *($p<0.001$)*, which was not expected, but seems logical considering the variability of sensory-motor ability between individuals.

It can be seen from Figure 7 (b), that in the range from 10 – 30 mmHg, 2 measures are lower for the *U* condition, while in the range from 40 – 60 mmHg, 2 measures are higher for the *U* condition. Two post-hoc tests on the effect of kinematic setting over the two pressure ranges confirmed that in the range from 10 – 30 mmHg subjects perform better in the *U* configuration *($p<0.001$)* whereas in the range from 40 – 60 mmHg they perform better in *L* configuration *($p<0.001$)*.

Thus, we can state that less interface load leads to better tracking performance if the attachment pressure of the exoskeleton on the human arm is low and that more interface load leads to better tracking performance if the attachment setting is overall stiff. To understand this seeming controversy, we show in [9] that humans prefer coherent behaviour of a mechanism. In [6] and [9] we furthermore showed that a low attachment pressure in the range from 10 – 30 mmHg is generally preferred for this task for the reason of higher experienced feeling of comfort.

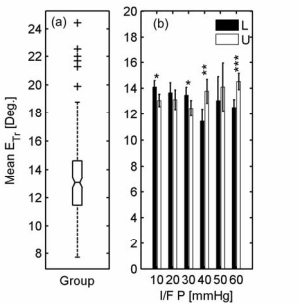

Figure 7. Total tracking error E_{Tr} of the group in (a) and in dependence of interface pressure factor (I/F P) and kinematic setting factor (*L, U*) in (b).

3.3 Available Voluntary Range of Motion

The kinematic setting variation affects the available range of motion. In Figure 8 (a), a full spectrum of the target and tracking signals is shown. It can be seen how often *(s_v)* the multisine target signal *v* and the subject's tracking signals in *L* or *U* kinematic configuration ($s_{\beta L}$ and $s_{\beta U}$ respectively) resided within one of the nine bins of elbow workspace α during the experiments (range *R(v)=R(α)*). In Figure 8 (b), the group mean of the voluntary range of motion R_β for both kinematic configurations is shown, in percent of the target signal *v* over the workspace.

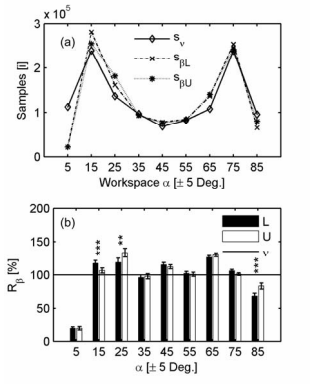

Figure 8. Range of motion R_β available with exoskeleton depending on kinematic configuration (*L*, *U*). In (a) via total number of samples lying within same angle bin than reference signal. In (b) as percent of reference signal reached.

It can be seen that on both stroke-ends, the subjects reached the target signal substantially less than 100 %. While in the range of 0 – 10 Deg., the subjects reach the target signal equally often for the two kinematic configurations, there is a significant difference towards the 80 – 90 Deg. stroke end. The subjects reach the far stroke end about 20 % more often (83.4 % versus 68.2 %) in the *U* kinematic configuration than in *L* configuration *($p<0.001$)*. Equally, the kinematic setting affects the range of motion in the mid-range of the workspace, however, subjects can anyway reach 100 % of the tracking signal in both conditions. Only the overshoot over the target signal is affected and the differences are less profound. These results, combined with the graph shown in Figure 4 further underline the statement that the passive joints act to remove peak loads that are created otherwise near the stroke ends.

3.4 Motion of the Passive Compensation Joints

The linear passive compensation joint d_{lin} of the exoskeleton operated within a range of 0 – 35 mm in the *U* trials. The rotary compensation joint Θ_{rot} operated within a range of – 11 to +25 Degrees. Figure 9 depicts the mean motion of d_{lin} in (a) and the motion of Θ_{rot} in (b), over all trials for the entire subject group. From Figure 9 it can be clearly seen how the movement of the compensation joints peaks near the stroke-ends. This underlines the fact that force is created mainly there in *locked* configuration.

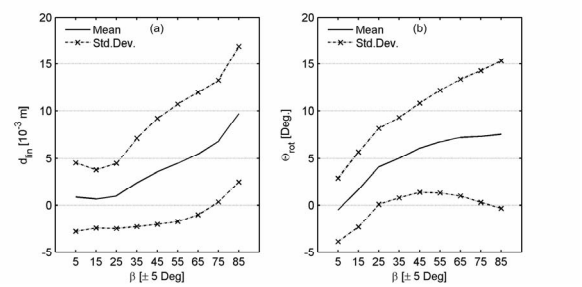

Figure 9. Motion in the offset compensation joints of the exoskeleton. Linear compensation joint motion in (a), and rotary compensation joint motion in (b)

4 DISCUSSION

This experiment, for the first time, quantified the effects of joint misalignment and kinematic exoskeleton configuration on interface load creation and objective performance metrics in a typical signal tracking task.

The results presented above show that despite an initially accurate alignment between the human elbow joint and the exoskeleton articulation, offsets still occurred during movement. Such offsets are shown to be in the range of ± 10 cm. Consequently, slip of the mechanism must have occurred or internal strain inside the exoskeleton structure must have acted to amplify the small joint offsets that possibly still existed at the start of the experiments. It is interesting to note, that not even with the highest attachment pressures of 60 mmHg, this slip or magnification of offsets was prevented. It is shown by the results above, that the joint center of rotation offsets are responsible for the creation of large interface forces. They almost reach up to 230 N and 1.5 Nm if the passive joints are blocked. Considering the fact that the exoskeleton was not even actuated, these are significant disturbance forces. Their magnitude lies in the same range than typical feedback forces and torques for haptic devices. It is important to stress that the exoskeleton was perceived as 'fitting well' to the users, and that there was no 'external' reason to believe that the device was ill-designed. When its compensation joints are locked, the EXARM emulates the designs of most other available exoskeletons.

While the results show strong evidence that interaction forces are responsible for a restriction of the voluntary range of motion, the influence on perceived user comfort was not analyzed in this paper. In [6], a dedicated analysis of the same parameter's influence on subjective performance is provided. Therefore, the results presented in [6] are important to put all elements of this investigation into perspective. Nevertheless, it seems important already from the shear magnitude of forces reported here, to try reducing them as much as possible.

We have shown by the results above, that the inclusion of passive compensation joints available in the EXARM are a good solution – as expected. The *unlocked* kinematic setting contributed to a significant reduction of such interface loads and to a larger available range of motion. The reduction of peak forces was shown to primarily happen near the stroke-ends.

Besides the quantification of offsets, attachment stiffness and typical interface loads during movement presented in this work, the experiment has also shown how the application of an analytical physical human-robot interaction model can be employed to (1) understand the causes of interface load creation and to (2) optimize the functioning of the passive joints of the exoskeleton. The topic of optimization was not treated largely here, but will be the topic of future discourses.

Nevertheless, we can already clearly state that without an analytical framework, the effects of offsets to interface load could not have been explained. Also, the estimation of attachment stiffness would have been difficult. The provision of numerical values for the attachment stiffness is deemed useful for modeling of teleoperation networks, as is necessary if an exoskeleton is to be used as haptic device.

5 CONCLUSIONS

(1) Offsets between the axes of rotation of a human and a robot, can easily be in the order of ± 10 cm in various directions, even if, at the start of movement, the two axes are well aligned. (2) Such offsets appear to be created by slip and amplification of initial offsets that are still apparent after visual alignment between exoskeleton and human joints. (3) Such offsets are the cause of large interaction loads between exoskeleton and human limbs. During movement, interface forces can reach up to 230 N along the axis of the human limb and interaction torques around the attachment cuffs can be created that rise up to about 1.46 Nm. (4) In conventionally designed exoskeletons without compensation joints, these interaction loads limit the voluntary range of motion near the stroke ends. (5) An exoskeleton that features passive compensation joints can lower such interaction forces by 70 % and the torques by at least 60 %. Additionally, passive compensation joints can permit a 20 % larger range of motion in the far stroke-ends of movement. (6) In order for an exoskeleton device with passive joints to work optimally, its passive joints must feature sufficient stroke margin in both directions over the entire workspace. (7) An exoskeleton with passive compensation joints can be called "ergonomic". (8) Typically, the attachment stiffness between an exoskeleton and the human limb is within 273 N/m ± 46 N/m as identified from measured interface forces from experiments with 14 test persons.

REFERENCES

[1] A. Frisoli, F. Rocchi, S. Marcheschi, A. Dettori, F. Salsedo, and M. Bergamasco, "A New Force-Feedback Arm Exoskeleton for Haptic Interaction in Virtual Environments," in Eurohaptics Conference and Symposium on Haptic Interfaces for Virtual Environment and Teleoperator Systems. First joint World Haptics Conference, Pisa, 2005, pp. 195-201.

[2] A. Schiele, M. D. Bartolomei, and F. v. d. Helm, "Towards Intuitive Control of Space Robots: A Ground Development Facility with Exoskeleton," in IEEE/RSJ International Conference on Intelligent Robots and Systems (IROS), Beijing, 2006, pp. 1396-1401.

[3] A. Zoss and H. Kazerooni, "Design of Electrically Actuated Lower Extremity Exoskeleton," Advanced Robotics, vol. 20, pp. 967-988, 2006.

[4] R. Riener, T. Nef, and G. Colombo, "Robot-aided neurorehabilitation of the upper extremities," Medical and Biolocial Engineering and Computing, vol. 43, pp. 2-10, February 2005.

[5] R. Alami, A. Albu-Schaeffer, A. Bicchi, R. Bischoff, R. Chatila, A. D. Luca, A. D. Santis, G. Giralt, J. Guiochet, G. Hirzinger, F. Ingrand, V. Lippiello, R. Mattone, D. Powell, S. Sen, B. Siciliano, G. Tonietti, and L. Villani, "Safe and Dependable Physical Human-Robot Interaction in Anthropic Domains: State of the Art and Challenges," in presented at: IEEE International Conference on Intelligent Robots and Systems Beijing, China: IEEE, 2006.

[6] A. Schiele, "Fundamentals of Ergonomic Exoskeleton Robots", Ph.D. Thesis, Delft University of Technology, 2008, available freely from: www.library.tudelft.nl

[7] A. Schiele and F. v. d. Helm, "Kinematic Design to Improve Ergonomics in Human Machine Interaction," IEEE Transactions on Neural Systems and Rehabilitation Engineering, vol. 14(2), pp. 456-469, 2006.

[8] A. Schiele, "An Explicit Model to predict and Interpret Constraint Force Creation in pHRI with Exoskeletons," in IEEE International Conference on Robotics and Automation, Pasadena, 2008, pp. 1324-1330.

[9] A. Schiele, "Case study: The ergonomic EXARM exoskeleton," in Wearable robots: Biomechatronic exoskeletons, J. L. Pons, Ed.: John Wiley & Sons, 2008, pp. 248-255.